

01 Apr 2023

Numerical Study of Turbulent Flow and Heat Transfer in a Novel Design of Serpentine Channel Coupled with D-Shaped Jaggedness using Hybrid Nanofluid

Raditun E. Ratul

Farid Ahmed

Syed B. Alam

Missouri University of Science and Technology, alams@mst.edu

Md Rezwatul Karim

et. al. For a complete list of authors, see https://scholarsmine.mst.edu/nuclear_facwork/536

Follow this and additional works at: https://scholarsmine.mst.edu/nuclear_facwork



Part of the [Nuclear Engineering Commons](#)

Recommended Citation

R. E. Ratul et al., "Numerical Study of Turbulent Flow and Heat Transfer in a Novel Design of Serpentine Channel Coupled with D-Shaped Jaggedness using Hybrid Nanofluid," *Alexandria Engineering Journal*, vol. 68, pp. 647 - 663, Elsevier, Apr 2023.

The definitive version is available at <https://doi.org/10.1016/j.aej.2023.01.061>



This work is licensed under a [Creative Commons Attribution-Noncommercial-No Derivative Works 4.0 License](#).

This Article - Journal is brought to you for free and open access by Scholars' Mine. It has been accepted for inclusion in Nuclear Engineering and Radiation Science Faculty Research & Creative Works by an authorized administrator of Scholars' Mine. This work is protected by U. S. Copyright Law. Unauthorized use including reproduction for redistribution requires the permission of the copyright holder. For more information, please contact scholarsmine@mst.edu.



ORIGINAL ARTICLE

Numerical study of turbulent flow and heat transfer in a novel design of serpentine channel coupled with D-shaped jaggedness using hybrid nanofluid



Raditun E. Ratul^a, Farid Ahmed^b, Syed Alam^c, Md. Rezwanul Karim^a,
Arafat A. Bhuiyan^{a,*}

^a Department of Mechanical and Production Engineering, Islamic University of Technology (IUT), Board Bazar, Gazipur 1704, Bangladesh

^b Department of Nuclear Engineering, North Carolina State University, Raleigh, NC, USA

^c Nuclear Engineering and Radiation Science, Missouri University of Science and Technology, Rolla, USA

Received 10 October 2022; revised 16 January 2023; accepted 27 January 2023

KEYWORDS

CFD;
Serpentine channel;
Heat transfer enhancement;
Hybrid nanofluid;
Dimple;
PEC

Abstract This study aimed to examine numerically the effects of a dimpled surface over a mini-channel heat exchanger on the flow characteristics and heat transfer across a serpentine channel with a uniform rectangular cross-section. The dimples were arranged in parallel with a spanwise (y/d) distance of 3.125 and streamwise (x/d) distance of 11.25 along just one side of the serpentine channel's surface. Turbulent flow regime with Reynolds number ranging from 5×10^3 to 20×10^3 in the channel with the surface modification was studied using water and various volume concentrations ($\phi = 0.1\%$, 0.33% , 0.75% , 1%) of Al_2O_3 -Cu/water hybrid nanofluid as the coolant to achieve a three-step passive heat transfer enhancement. Applying the Finite Volume Method (FVM), RNG k- ϵ turbulence model, and a constant heat flux of 50 kW/m^2 , simulations were run assuming the mixture of Al_2O_3 -Cu nanoparticles homogenous using ANSYS 2020 R1. The second-order upwind approach is used for approximation of solution and discretization with SIMPLE pressure-velocity coupling. Taking heat transfer increment and pressure drop penalty into consideration, the dimpled serpentine channel provides a 1.47-times improvement in thermal efficiency using water as the coolant, and the dimpled channel with 1% vol. Al_2O_3 -Cu/water nanofluid enhanced thermal efficiency by a remarkable maximum of 2.67-times at $\text{Re} 5 \times 10^3$. The study also indicates that thermal efficiency increased with an increasing volume concentration of the nanofluid and increment in thermal efficiency gradually decreased as the Re increased.

© 2023 THE AUTHORS. Published by Elsevier BV on behalf of Faculty of Engineering, Alexandria University. This is an open access article under the CC BY-NC-ND license (<http://creativecommons.org/licenses/by-nc-nd/4.0/>).

* Corresponding author.

E-mail address: arafat@iut-dhaka.edu (A.A. Bhuiyan).

Peer review under responsibility of Faculty of Engineering, Alexandria University.

<https://doi.org/10.1016/j.aej.2023.01.061>

1110-0168 © 2023 THE AUTHORS. Published by Elsevier BV on behalf of Faculty of Engineering, Alexandria University. This is an open access article under the CC BY-NC-ND license (<http://creativecommons.org/licenses/by-nc-nd/4.0/>).

Nomenclature

CFD	Computational Fluid Dynamics	W	Watt
Re	Reynolds number	vol. %	volume concentration (%)
FVM	Finite Volume Method	wt%	weight concentration (%)
TKE	Turbulent Kinetic Energy	ΔP	Pressure Drop
Pr	Prandtl number	ρ	Density
e/d	Dimple depth to dimple diameter ratio	φ	Volume fraction (%)
HTC	Heat transfer coefficient		
x/d	Stream wise spacing		
y/d	Span wise spacing		
PEC	Performance Evaluation Criterion	<i>Subscripts</i>	
TI	Turbulent Intensity	i, j, k	tensor index
Nu	Nusselt number	rs:	Rough Surface
v	Velocity (m/s)	ss:	Smooth Surface
T	Temperature (K)	nf:	Nanofluid
Dh	Hydraulic diameter	bf:	Base Fluid
\dot{Q}	Wall heat flux (W/m^2)	bulk:	Bulk
C_p	Specific heat of fluid ($J/kg K$)	w:	Wall
P	pressure (N/m^2)	l:	Flow direction
k	Thermal conductivity ($W m^{-1} K^{-1}$)	0	Initial value
μ	Dynamic viscosity ($(Ns)/m^2$)	avg:	Averaged
		u, v, and w	Velocity components along x, y, and z directions respectively

1. Introduction

One of the biggest technological challenges in industries is improving the thermal performance of various devices and machines. Effective cooling is extremely desirable for assuring reliable or stable thermal performance, which raises the need for creating energy-efficient solutions to promote appropriate heat transfer while keeping installation and maintenance costs low. Active and passive methods for improving heat transfer rates are quite popular in the industry. Active methods involve coolant pulsation, magnetic or electrostatic fields, etc. [1–3]. Active methods require more power, which can inconvenience industries. Passive methods are gaining popularity due to lower costs and maintenance. Passive heat transfer enhancements include using nanofluids, increasing surface area and fluid turbulence [4–6]. Increasing the length of the flowing channel by coiling or serpentineing it, introducing dimples, fins, ribs, different types of protrusions, and corrugations to increase surface roughness, inserting helical coiled wire, twisted tapes, etc. along the fluid flow direction are prominent passive methods for heat transfer enhancement [7–11]. Serpentine channels have innumerable applications in almost all engineering sectors and industries like the nuclear sector, chemical industries, solar collectors, HVAC and refrigeration systems, thermal engineering and power plants, etc. Due to the compact size, large heat transfer area and curvature effects serpentine channels are ideal for use as heat exchangers.

According to fluid dynamics dimples, protrusions, and other passive methods disrupt boundary layer formation [12,13]. This increases channel turbulence and heat transfer. Attaching flow fields for circulation and recirculation to the wall repeatedly and increasing the effective surface area improve thermal performance [14,15]. Again, the use of nanofluid in corrugated and crooked channels (helix-shaped, spiral, twisted, or serpentine-shaped) is a modern passive heat trans-

mission method [16–20]. Many applications and the immense significance of diverse technical thermal devices using nanofluid have come from these researches [21–24]. Porous channels are also quite often used as heat transfer media [25–27]. Using $\gamma-Al_2O_3-CuO$ water-based nanofluid, Bayoumi et al. [28] significantly improved the performance of cooling of an Intel Core i7 CPU, according to experimental and numerical results. The thermal performance of a double-pipe heat exchanger with a counter-flow mechanism employing Nitrogen-Doped Graphene (NDG) nanofluid was investigated experimentally and numerically by Goodarzi et al. [29–31]. The conclusion from this and similar studies performed was that increasing Reynolds number and nanomaterial loading increases heat transfer rate at a price of pressure drop. Studies are also conducted with micropolar fluids in different channels to understand their effect in linear and micro-rotation velocity [32,33].

Ajeel et al. [7] studied thermal performance and design parameters in a novel corrugated-curved channel with ZnO/water nanofluid and obtained a 2.57 times improvement in the thermal-hydraulic performance factor. They dealt with various geometric parameters like gap ratio, blockage ratio and pitch angle, and tests were carried out at the Reynolds number range of 8000–32000. Experiments were performed on Cu/water nanofluid flow and heat transfer in five different serpentine pipes with varied straight section lengths by M. Khoshvaght-Aliabadi et al. [34]. The Performance Evaluation Criterion value of 1.18 is attained by the 0.40 % wt. nanofluid in the serpentine channel with the configuration of low to high straight section lengths. The impact of innovative passive approaches on heat exchanger thermal performance was studied numerically by Feizabadi et al. [35] where varied lengths, twisted pitches, and serpentine pitches of Al_2O_3 /water nanofluid was employed in the investigation. The results revealed the impact of altering the straight length and volumetric concentration of nanoparticles on a twisted serpentine tube's thermal performance.

Abed et al. [36] experimentally analyzed the heat transfer and elastic turbulence impact in a serpentine channel with a square cross-section and obtained up to 200% and 380% increments in convective heat transfer for low and high polymer concentrated solutions respectively. However, they encountered about 3.3 times more pressure drop to achieve this increment.

Ajeel et al. [37,38] studied convective heat transfer in corrugated channels experimentally and numerically using SiO₂-water nanofluid. They found that in turbulent flow regimes, corrugation as well as using nanofluid significantly enhanced the heat transfer rate. They also proposed a novel type of trapezoidal corrugation channel which offered outstanding heat transfer enhancement when compared to a straight channel. Huminic et al. [39] demonstrated the significant influence of TiO₂/water and CuO/water nano-fluids on the entropy generation and thermal performance of helically coiled tube of tube heat exchangers by means of numerical approach and obtained that increasing particle loading results in an increase in Nusselt number and a decrease in entropy generation.

Perwez et al. [40] explored the influence of spherical dimpled surfaces and tear-drop in a rectangular channel with Reynolds numbers ranging from 14×10^3 to 65×10^3 using numerical and experimental means. Compared to spherical dimples, rectangular channels with teardrop-dimpled surfaces increased heat transmission by 17%. The thermo-hydraulic properties of a dimpled surface were investigated in an experimental investigation by Chen et al. [41] utilizing water as a coolant and forced turbulent flow in an annular channel. Heat transmission was increased to 137% from 25% in the investigation when a dimpled surface was used instead of a plain tube. Different types of artificial roughness, such as corrugated surfaces, dimpled surfaces, and helical wired coils were tested by Garcia et al. [42] in both turbulent and laminar conditions to determine the influence on flow. It was found that when Reynolds Number exceeds 2000, the dimpled surfaces outperform other examined roughness in terms of thermal performance. Bhattad and Sarkar [43,44] experimentally studied the thermal performance and exergy analysis of a plate heat exchanger using graphene - Al₂O₃ hybrid nanofluid. They obtained 25.36% enhancement in HTC as compared to the base fluid with 0.01% vol. concentration and with a particle volume ratio of 4:1. Al₂O₃-CuO/water hybrid nano-fluid was tested by Selvakumar et al. [45] in electronic heat sinks keeping the volumetric flow rate constant with deionized water to determine its performance. The authors found a 24.35% increment in heat transfer efficiency when using a hybrid nano-fluid with a 0.1% volumetric concentration. They also found that pumping power has to be increased by 12.61% to achieve an improvement of 11.74%. However, an evaluation of thermal efficiency was missing in their work which determines the credibility of the hybrid nano-fluid as a coolant. Bhattad et al. used various hybrid nanofluids with different concentrations in a plate heat exchanger and obtained significant improvement in thermal performance. In their studies they used brine based hybrid nanofluids [46,47], Al₂O₃-MWCNT [48], Al₂O₃-MgO [49]. All of these resulted in significant heat transfer enhancement, reduction of pumping power requirement, and lowering of heat transfer area.

The variation of thermal conductivity in an annulus is studied by Parvin et al. [50] using Al₂O₃/Water nanofluid. They

found that heat transfer enhancement occurs as the nanofluid concentration and the Prandtl number are raised. Sundar et al. [51] developed Al₂O₃-Cu nano-composite-based nano-fluids and obtained a 13.56% increase in heat transfer at Re 1750. The study showed the acceptance of the hybrid nano-fluid providing remarks on the thermal efficiency. However, the investigation was limited to the laminar flow regime. Hence, a detailed investigation is required to understand the behavior of Al₂O₃-Cu /water in a turbulent flow regime.

According to the discussed literature, it is obvious that hybrid nano-fluids, serpentine channels, and channel surface modifications considerably improved thermal efficiency. However, to the best of the authors' knowledge, numerically and experimentally not much work has been done using serpentine channels with surface modifications. Though hybrid nano-fluids are better performers than conventional nano-fluids in most cases and are a topic of current focus, little to no study has been conducted using hybrid nano-fluids in serpentine channels. Moreover, the investigations of both the global and local parameters for serpentine channels as well as hybrid nano-fluids are quite limited. The objective of this study is to compare heat transfer enhancement between various concentrations of a hybrid nano-fluid (Al₂O₃-Cu/water) in a novel serpentine channel with surface modification, i.e., dimple configuration. The goal is to develop a three-step passive method for heat transfer enhancement and to obtain the best-performing nanofluid among the test cases. Both local and global thermo-hydraulic characteristics are evaluated and compared in the study to understand the flow of hybrid nano-fluids and the effects of spherical dimples in a serpentine channel. The present study is divided into two segments. Firstly, an investigation of forced convection flow in a smooth serpentine channel and a dimpled serpentine channel using water as the working fluid is performed. Secondly, the comparative study between the nano-fluids is studied in the serpentine channel with hemispherical dimples. Al₂O₃-Cu/water at $\phi = 0.1\%$, 0.33% , 0.75% , and 1% are used in this study as the working fluid.

2. Thermo-physical properties of nano-fluid

Various classical models are used to calculate the thermophysical properties of a nanofluid. The models are modified slightly to obtain the theoretical properties of a hybrid nanofluid.

$$\rho_{nf} = \phi_p \rho_p + (1 - \phi_p) \rho_{bf} \quad (1)$$

This model takes the volume fraction and density of the nanoparticles and basefluid into account and is used to calculate the density of the nanofluid. For hybrid nanofluid, total volume fraction ϕ is the sum of the volume concentrations of the two types of nanoparticle constituents.

$$\phi_p = \phi_{Al_2O_3} + \phi_{Cu} \quad (2)$$

So, the density of hybrid nanofluid is found out from equation (3).

$$\rho_{mf} = \phi_{Al_2O_3} \rho_{Al_2O_3} + \phi_{Cu} \rho_{Cu} + (1 - \phi_p) \rho_{bf} \quad (3)$$

Equation (4) is used to calculate the heat capacity of nanofluids and equation (5) is modified to obtain the heat capacity of Al₂O₃/Cu hybrid nanofluid.

$$C_{nf} = \frac{\varphi_p \rho_p C_p + (1 - \varphi_p) \rho_{bf} C_{bf}}{\rho_{nf}} \quad (4)$$

$$C_{hmf} = \frac{\varphi_{Al_2O_3} \rho_{Al_2O_3} C_{Al_2O_3} + \varphi_{Cu} \rho_{Cu} C_{Cu} + (1 - \varphi_p) \rho_{bf} C_{bf}}{\rho_{hmf}} \quad (5)$$

Hamilton and Crosser [52] were the first ones to come up with the model to calculate the thermal conductivity of a nano-fluid which is shown in **Equation (6)**. The empirical shape factor, denoted by the letter n and ranging in value from 0.5 to 6.0, is used in this equation to take the influence of the particles' shapes into consideration. The sphericity of a particle, measured as the ratio of the particle's surface area to that of a sphere, is denoted by the form factor n , which is equal to 3ψ . Nanoparticles with a spherical shape have an n -value of 3.

$$\frac{k_{nf}}{k_{bf}} = \frac{k_p + (n - 1)k_{bf} - (n - 1)\varphi_p (k_{bf} - k_p)}{k_p + (n - 1)k_{bf} + \varphi_p (k_{bf} - k_p)} \quad (6)$$

Putting the value of n in **equation (6)**, **equation (7)** is obtained.

$$\frac{k_{nf}}{k_{bf}} = \frac{k_p + 2k_{bf} - 2\varphi_p (k_{bf} - k_p)}{k_p + 2k_{bf} + \varphi_p (k_{bf} - k_p)} \quad (7)$$

Takabi et al. [53] discussed the most commonly used models to calculate the viscosity of a hybrid nanofluid. The mentioned models are.

Einstein Model:

$$\mu_{nf} = \mu_{bf}(1 + K_1\varphi) \quad (8)$$

Brinkman Model:

$$\mu_{nf} = \frac{\mu_{bf}}{(1 - \varphi)^{2.5}} \quad (9)$$

Batchelor Model:

$$\mu_{nf} = \mu(1 + K_1\varphi + K_2\varphi^2) \quad (10)$$

Where $K_1 = 2.5$ and $K_2 = 6$. K_2 quantifies the deviation of the nanofluid from the suspensions' very dilute limit. This value of K_2 is obtained by allowing a superimposed Brownian motion.

According to Suresh et al. [54] these models provide values only acceptable for nanofluids with lower concentrations. So, to achieve more accuracy in the present study, the experimental values of density, heat capacity, thermal conductivity and viscosity for $\varphi = 0.1\%$, 0.33% , 0.75% and 1% Al_2O_3/Cu are taken from Saghir et al. [55].

Although nanofluid is originally a two-phase mixture because of the presence of solid particles in the base fluid; still, the physics of conventional two-phase flow may not apply to nanofluid [56]. As nanofluids are composed of nanosized particles and also are of very low concentration, they behave like a fluid rather than a combination of the base fluid and nanoparticles (solid-fluid phase) [57]. Xuan and Roetzel [58] came up with a homogeneous model where the convective heat transport theory equations for fluids were extended to nanofluids. This shows the fact that if the characteristics of base fluids are changed to those of nanofluids, the traditional Nusselt number correlations would be suitable for usage in nanofluids for lower volume concentrations. Nevertheless, many more studies were conducted considering the nanoparticle mixture as a homogenous mixture and the flow approach as a single-phase, and the results obtained are aligned with the results of experimental studies with precision [59,60]. On

the other hand, various studies are also done using the two-phase method [61,62]. Bhattad et al. compared and found that the Discrete phase model showed better results compared to the homogenous method. When the objective is to analyze the particle behavior from the Lagrangian point of view a discrete phase model is usually used. However, using Al_2O_3 /water as a working fluid the two-phase Mixture Model was shown to be less accurate in predicting the nano-fluid thermo-hydraulic behavior [63–65]. A maximum disparity of 5.9% was discovered between the Discrete Phase Model and single-phase approaches in these investigations. Since the experimental findings correspond well with the numerical assumptions of the different investigations [66–69], the study proposed adopting a single-phase technique with temperature-independent thermo-physical characteristics for nano-fluids with less than 1.5% volume fraction, provided the best feasible precision in thermo-physical properties is attained for nano-fluids. **Table 1** exhibits the thermo-physical properties of the coolants used in the study (see **Table 2**).

3. Computational geometry

The flow channel which is used in the investigation of the present study is a serpentine channel with a uniform rectangular cross-section. It has three turns with a mean radius of 42.5, 57.5, and 42.5 respectively. The mean length of the channel is taken to be 2577.68 mm and the width and the height of the channel cross-section are 15 mm and 50 mm respectively. Hydraulic diameter (D_h) is measured to be 23.07 mm and it is considered constant throughout the channel. The diameter (d) of the hemispherical dimple on the uniform channel is 8 mm and thus has a depth of 4 mm. The dimples were set in a parallel arrangement with a spanwise (y/d) distance of 3.125 and streamwise distance (x/d) of 11.25 at a stretch up to each curve of the serpentine channel along only one side of its surface. The investigated study's geometrical configuration is evinced in **Fig. 1**.

4. Mathematical modeling

4.1. Numerical investigation assumptions

- 1) During the numerical investigations, the working fluid is assumed to be a Newtonian fluid and consequently, the stress to strain ratio is considered constant.
- 2) As the coolants are considered as Newtonian fluid, the viscosity of the coolants is assumed to be shear rate independent [70].
- 3) The working thermo-fluids are considered to be incompressible fluids.
- 4) The combination of nanoparticles and base fluid is regarded to be a homogenous mixture since the particles are dispersed uniformly throughout the liquid [71,72]. So, the solid nanoparticle's velocity was considered to be the same as the velocity of the base fluid.
- 5) Numerical simulations were carried out on the assumption of a steady state condition.

The simulations are run in a turbulent flow regime with four different Re in gradually increasing order from 5×10^3 to 20×10^3 . To solve the 3D Navier-Stokes equation Finite Volume Method was used.

Table 1 Thermo-physical properties of working fluids at $T = 303$ K; reproduced from Saghir et al. [55].

Fluid Name	Density (kg/m ³)	Viscosity (Pa.s)	Thermal Conductivity (Wm ⁻¹ K ⁻¹)	Heat Capacity (J/kg.K)
Water	995.7	0.0008015	0.614	4174
0.1%vol. Al ₂ O ₃ -Cu	1001.3	0.00097	0.6201	4176.83
0.33%vol. Al ₂ O ₃ -Cu	1006.64	0.0011	0.6312	4143.5184
0.75%vol. Al ₂ O ₃ -Cu	1017.37	0.00139	0.6491	4095.5
1% vol. Al ₂ O ₃ -Cu	1023.75	0.0016	0.65727	4067.415

Table 2 Comparison of Change in Turbulence Intensity in terms of Nusselt Number and Pressure drop.

Turbulence Intensity (%)	Nu	ΔP [Pa]
5%	305.26	752.39
10%	310.46	736.26

4.2. Governing equations of the present study

The governing equations of the present study basing on the assumptions are.

Continuity Equation:

$$\frac{\partial}{\partial x_i}(\rho v_i) = 0 \quad (11)$$

Momentum Equation:

x component:

$$\rho F_i - \frac{\partial p}{\partial x_i} + \mu \left(\frac{\partial^2 v_i}{\partial x_i^2} + \frac{\partial^2 v_i}{\partial x_j^2} + \frac{\partial^2 v_i}{\partial x_w^2} \right) = \rho \frac{dv_i}{dt} \quad (12)$$

y component:

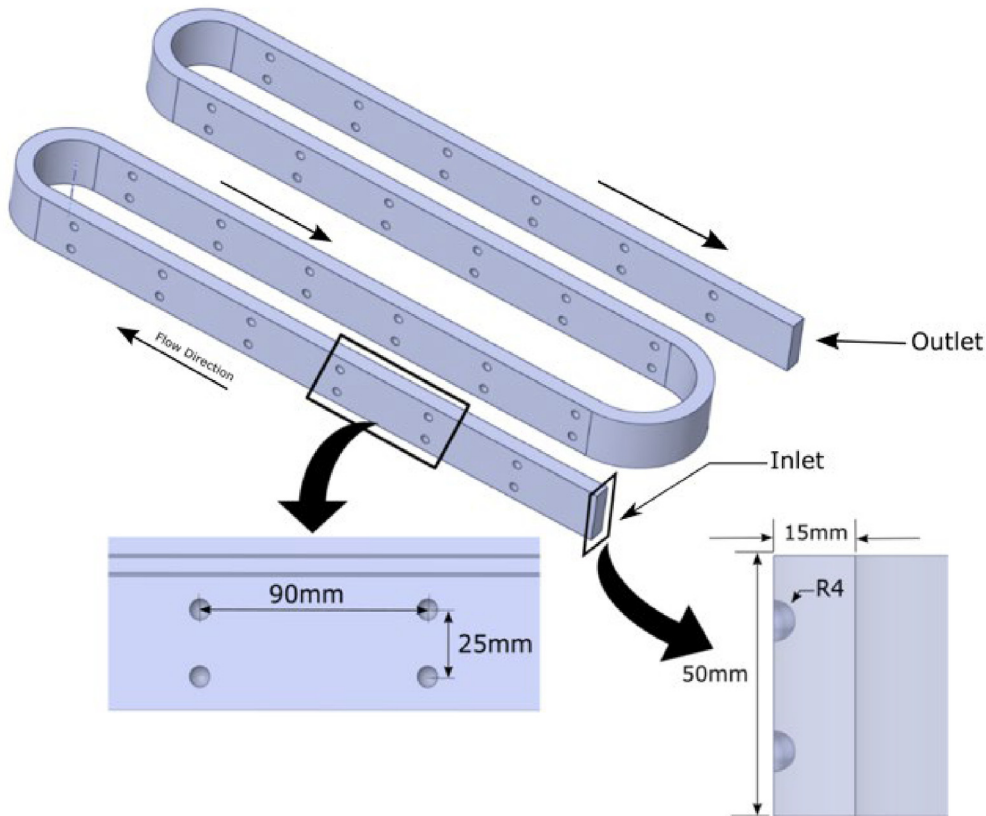
$$\rho F_j - \frac{\partial p}{\partial x_j} + \mu \left(\frac{\partial^2 v_j}{\partial x_i^2} + \frac{\partial^2 v_j}{\partial x_j^2} + \frac{\partial^2 v_j}{\partial x_w^2} \right) = \rho \frac{dv_j}{dt} \quad (13)$$

z component:

$$\rho F_w - \frac{\partial p}{\partial x_w} + \mu \left(\frac{\partial^2 v_w}{\partial x_i^2} + \frac{\partial^2 v_w}{\partial x_j^2} + \frac{\partial^2 v_w}{\partial x_w^2} \right) = \rho \frac{dv_w}{dt} \quad (14)$$

Energy Equation:

$$\frac{\partial T}{\partial \tau} + v_i \frac{\partial T}{\partial x_i} + v_j \frac{\partial T}{\partial x_j} + v_w \frac{\partial T}{\partial x_w} = \frac{\lambda}{\rho c_p} \left(v_i \frac{\partial^2 T}{\partial x_i^2} + v_j \frac{\partial^2 T}{\partial x_j^2} + v_w \frac{\partial^2 T}{\partial x_w^2} \right) \quad (15)$$


Fig. 1 Geometrical configuration of the computational domain.

4.3. Turbulence model selection

The precision of the complex geometry model's analysis is largely dependent on the selection of a suitable turbulence model. It is important to consider flow physics, as well as the level of precision, which is necessary while selecting a relevant model for a specific problem. Kumar et al. [73] studied the fluctuation of the Nusselt number with Re for several turbulence models with the findings from the Dittus-Boelter equation for a smooth walled channel. They found that the equation results and the results from the RNG k- ϵ model were very close. According to Yadigaroglu et al. [74], in terms of performance, the k-epsilon model was not satisfactory in predicting turbulent flow dynamics in flow regions with narrow widths. In the investigation of the thermal-hydraulic behavior, Rahimi-Esbo et al. [75] developed a new modified model of the SST k- ϵ . The use of a precise, distinctive model for the analysis of this kind of flow pattern is then demonstrated to have some advantages. Time and memory space is highly prioritized during ANSYS simulation and modeling and a model named Reynolds Stress Equation Model (RSM) turbulence model, needs more time and data with increasing computational accuracy [76]. It uses 15%-20% more memory and around 50% to 60% more time in a single iteration than the k- ϵ and k- ω turbulence models. Since time and memory space are highly prioritized during ANSYS simulation and modeling, the RSM turbulence model is avoided here for the optimized result. Ahmad et al [77,78] used the RNG k- ϵ model to examine the enhancement of heat transfer of turbulent nanofluid forced flow in a duct introducing a triangular rib. This turbulence model was developed by the use of a rigorous statistical approach known as the renormalization group RNG theory [79]. This theory was obtained from the Navier-Stokes equations by filtering. The Boussinesq hypothesis forms the basis for the RNG k- ϵ model, which links the Reynolds tensor to the gradient of the mean velocity, turbulent viscosity, and turbulent kinetic energy. When compared to the normal k- ϵ model, the RNG model's inclusion of refinements results in a

significant improvement in the accuracy of the prediction of quickly strained flow. Unlike the Standard k- ϵ model, the RNG k- ϵ model also provides better results for a wide range of Reynolds numbers because this theory gives a differential formula that has been analytically derived and it considers the low Reynolds number effect too. Because of these benefits, the RNG k- ϵ model is superior to the Standard k- ϵ model in terms of accuracy and dependability for a greater variety of flow conditions [80,81]. Hence, RNG k- ϵ model was implemented for numerical simulations of the present study. The model is expressed by the equations (16) and (17) [82].

For $0.5 < Pr < 120$ and $6.0 \times 10^3 < Re < 1.0 \times 10^7$,

$$\frac{\partial}{\partial t}(\rho k) + \frac{dy}{dx_i}(\rho \epsilon u_i) = \frac{d}{dx_j} \left(a_k \mu_{eff} \frac{dk}{dx_j} \right) + G_k + G_b - \rho \epsilon - Y_M + S_k \quad (16)$$

$$\frac{\partial}{\partial t}(\rho \epsilon) + \frac{dy}{dx_i}(\rho \epsilon u_i) = \frac{d}{dx_j} \left(a_k \mu_{eff} \frac{d\epsilon}{dx_j} \right) + C_{1\epsilon} \frac{\epsilon}{k} (G_k + C_{3\epsilon} G_b) - C_{2\epsilon} \rho \frac{\epsilon^2}{k} - R_\epsilon + S_\epsilon \quad (17)$$

Here, $C_{1\epsilon}$, and $C_{2\epsilon}$ are developed from the theory as model constants. The values of these constants are taken as 1.44 and 1.92 respectively.

5. Grid sensitivity analysis

The precision of numerical simulation is dependent on how the grid is made for the fluid domain. The numerical calculations are performed using FVM by ANSYS Fluent. In FVM, the generation of grids across the geometry is crucial for solution convergence. Tetrahedral meshes were constructed over the serpentine channel with dimples with standard wall treatment. Near the wall, boundary layers were developed to accurately obtain the flow separations and thermal gradient. 13 inflation layers were added to obtain precise results near the wall surface as shown in Fig. 2 (a). Again, the element size and the

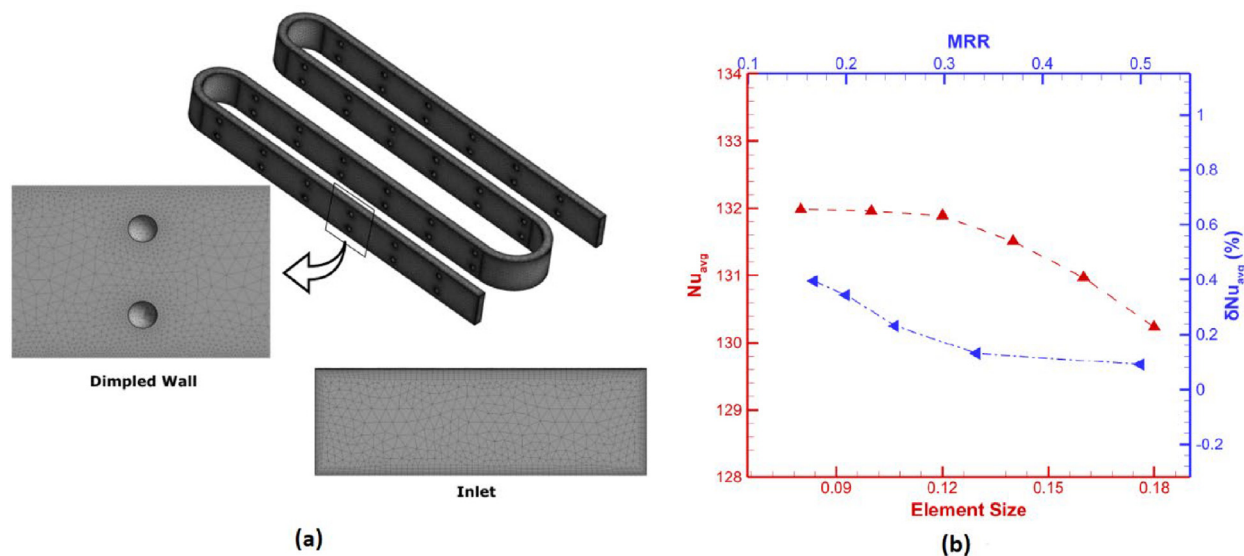


Fig. 2 (a) Grid Used (b) Sensitivity Analysis- MRR variation plot.

number of nodes have a significant role in predicting the numerical outcomes. Hence, the assessment of optimized mesh using the mesh independence test is required. By varying element size in accordance with the meshes' degree of refinement, the fluctuation of Nu was recorded. Fig. 2 (b) demonstrates the variation of Nu with element size. The varies significantly when the element size is 0.18 and 0.16. The value of Nu begins to become stable from element size 0.12 mm and remains almost steady for 0.1 mm and 0.08 mm. Since the magnitude of Nu does not vary considerably with decreasing element size, the computational domain mesh with 0.1 mm element size was chosen for the study. Mesh Refinement Ratio (MRR) is the ratio between the fluid domain's initial cell size and the final cell size, which is used to determine the increase in the node number and element size. Several MRRs were examined to comprehend grid independence, and Fig. 2 (b) also illustrates the change in averaged Nusselt number with respect to MRR. As the MRR value is increased the change in averaged Nusselt number gradually decreased and became stabilized. Fig. 2 (b) reveals that the MRR value of 0.5 provides the best estimation of Nu_{avg} with an error of only 0.09%. The chosen mesh model is represented in Fig. 2 (a) and selected for simulations of this study. In total there are 20,23,416 nodes and 45,92,864 elements in the selected mesh model.

6. Boundary conditions and data reduction

All the simulations were performed using a steady and uniform heat flux of $50\text{KW}/\text{m}^2$ on all the surfaces of the serpentine channel. Turbulent flow regime was studied with Re ranging from 5×10^3 to 20×10^3 with an interval of 5×10^3 . The inlet temperature for water and nanofluid was maintained at $T_0 = 303\text{K}$ and the gauge pressure at the outlet was kept at 0 Pa. Implicit solver was selected for solving the governing equations. The application of pressure-velocity coupling was carried out using SIMPLE algorithm, and then normal pressure interpolation was carried out. As the convergence criteria, for continuity and momentum equations, the Root Mean Square (RMS) value was set to 10^6 and for energy, the corresponding value was set to 10^9 . ANSYS 2020 R1 was used for performing all the simulations of the study.

At inlet-

$$T = T_{in} = 303k$$

$$V_{radial} = V_{tangential} = 0; V_{axial} = V_{in} \text{ (obtained from Re).}$$

At Wall-

$$V_{radial} = V_{tangential} = V_{axial} = 0$$

$$\dot{Q} = 50\text{KW}/\text{m}^2$$

At Outlet-

$$\frac{\delta V_{tangential}}{\delta \tau} = \frac{\delta V_{axial}}{\delta \tau} = 0; \frac{\delta T}{\delta \tau} = 0; \tau = \text{Flow Length.}$$

At Solid-fluid interface-

$$V_{tangential} = V_{axial} = 0; -k \frac{\delta T}{\delta r} = \dot{Q} = 0$$

Equation (19) was used as the formula for the Reynolds number. Corresponding to the Reynolds number, the velocity of the coolant was calculated using this equation. Here, v is the inlet velocity, ρ is the density of the coolant, μ stands for the viscosity of the coolant and D_h is the hydraulic length of the geometry. The value of D_h is calculated to be 23.07 mm from equation (18).

$$D_h = \frac{4.a.b}{a+b} \quad (18)$$

Here, a and b are the width and height of the rectangular cross section of the channel.

$$Re = \frac{\rho v D_h}{\mu} \quad (19)$$

$$h = \frac{\dot{Q}}{A(T_w - T_{bulk})} \quad (20)$$

The heat transfer coefficient was calculated using equation (20), where \dot{Q} represents the constant heat flux, A is the heat transfer area, and T_w is the wall temperature [14].

Equation (21) was used for calculating the fluid's bulk temperature. V_m is the maximum velocity along the channel length whereas τ_w represents the shear stress at the wall.

$$T_{bulk}(l) = T_w(l) + \frac{\dot{Q} V_m}{\tau_w C_p} \quad (21)$$

$$h_{avg} = \frac{1}{L} \int_0^L h(l) dl \quad (22)$$

The average heat transfer coefficient of the channel was obtained from equation (22) where L represents the total length of the flow channel. [14].

The average Nusselt number was calculated using equation (23).

$$Nu_{avg} = \frac{h_{avg} D_h}{k_0} \quad (23)$$

The friction factor was calculated using equation (24) where ΔP_{avg} is the average pressure drop along the length of the channel [10].

$$f = \frac{2\Delta P_{avg} D_h}{4\rho L v^2} \quad (24)$$

7. Data validation

Dittus-Boelter correlation [83] was given for a smooth straight channel with a circular cross-section. Equation (25) and equation (26) show the correlation of Nusselt number and Friction Factor respectively. However, these correlations are not valid for the case of the present study as the used channel is a serpentine channel with a rectangular cross-section.

$$Nu = 0.024 Re^{0.8} Pr^{0.4} \quad (25)$$

$$0.5 < Pr < 120; 6.0 \times 10^3 < Re < 1.0 \times 10^7$$

$$f = \frac{0.3164}{Re^{0.25}} \quad (26)$$

For dimpled channels, Maithani and Kumar [84] proposed correlations for Nusselt number and friction factor. Equation (27) and equation (28) are the correlations proposed by them. But as the correlations are for dimpled straight channels with circular cross-sections, the correlations are not applicable to this study.

$$Nu = 2.98 \times 10^{-3} Re^{0.9899} \left(\frac{y}{d}\right)^{1.3085} * \exp(-2.48 \ln\left(\frac{x}{d}\right)^2 \left(\frac{x}{d}\right)^{-0.1}}$$

$$*exp(-0.004ln(\frac{x}{d})^2 (\frac{e}{d})^{0.0998}) * exp(-2.385(\frac{e}{d})^2) \quad (27)$$

$$f = 366.46Re^{-1.068} \frac{y^{0.6351}}{d} exp(-0.1641ln(\frac{x}{d})^2) * (\frac{y}{d})^{1.4643} * exp(0.2968ln(\frac{y}{d})^2 (\frac{e}{d})^{0.1047}) * exp(-0.6009ln(\frac{e}{d})^2) \quad (28)$$

For the validation of the study, at first, the smooth serpentine channel was validated by comparing the results with the experimental correlations produced for Nu_{avg} by Karale et al. [85]. They used a serpentine channel made up of 10 units to conduct flow and heat transfer studies. The geometry was replicated and simulation was carried out with the same boundary conditions and specified mesh configurations of the present study and water with an inlet temperature of 298 K was used as the working fluid. Fig. 3(a) shows the comparison between the present study and the experimental values obtained by Karale et al. The Figure demonstrates that the numerical findings correspond well with the experimental data within a satisfactory margin of error. Nevertheless, the maximum deviation was 3.52% at Re 613.

Since similar studies incorporating dimples in the serpentine channel are not available and the authors are studying it for the first time, the validation of the serpentine dimple channel is accomplished also through a rectangular dimpled channel. The authors followed the experimental and numerical study investigated in a rectangular channel by Rao et al. [86]. To determine how different dimple configurations affect heat transmission and frictional flow over dimpled surfaces of varying dimple forms in turbulent flows, they carried out an experimental investigation and a computational analysis in a channel with a rectangular cross-section. Keeping the boundary conditions the same and following the specified mesh configurations of the present study and using water as the coolant, the simulation was performed. Fig. 3(b) displays the comparability between the Nusselt numbers of the present study with the numerical and experimental Nusselt numbers obtained from Rao et al [86]. A good agreement between the

Nusselt number obtained from the present study and the experimental and numerical Nusselt number values is noticed with a reasonable percentage of error. The maximum error obtained was with the experimental value and which is about 11.2% whereas the largest deviation seen for the CFD result was 5.05%. Both of the largest deviations were recorded for $Re 18.907 \times 10^3$.

Upon evaluating the aforementioned comparative studies, it is evident that the numerical results are quite close to the experimental investigation's results, which validate the numerical results presented for the spherical dimpled serpentine channel.

8. Results and discussion

This study compares the heat transfer coefficient, pressure drop, and thermal performance of serpentine smooth and dimple channels. Both local and global parameters were assessed in order to find the optimum result. The study is comprised of two segments. Firstly, the comparison of the thermal efficiency of the dimpled serpentine channel and smooth serpentine channel with rectangular cross-section was assessed. Secondly, investigations and comparisons of the thermal performances of the better channel with hybrid nanofluid of Al_2O_3 -Cu with water as base fluid are considered to find the best combination of passive heat transfer enhancement among the studied cases. Here, Al_2O_3 -Cu nanofluid with $\phi = 0.1\%$, 0.33% , 0.75% , and 1% volume fractions was studied in a dimpled channel considering single-phase approach. Turbulent flow in the channel was studied with varied Reynolds numbers from 5×10^3 to 20×10^3 with an interval of 5×10^3 .

8.1. Performance evaluation of serpentine channel with spherical dimple using water as coolant

8.1.1. Heat transfer coefficient (h_{avg})

Fig. 5 (a) shows the average HTC with respect to Re for a smooth and dimpled serpentine channel. From the graph, it

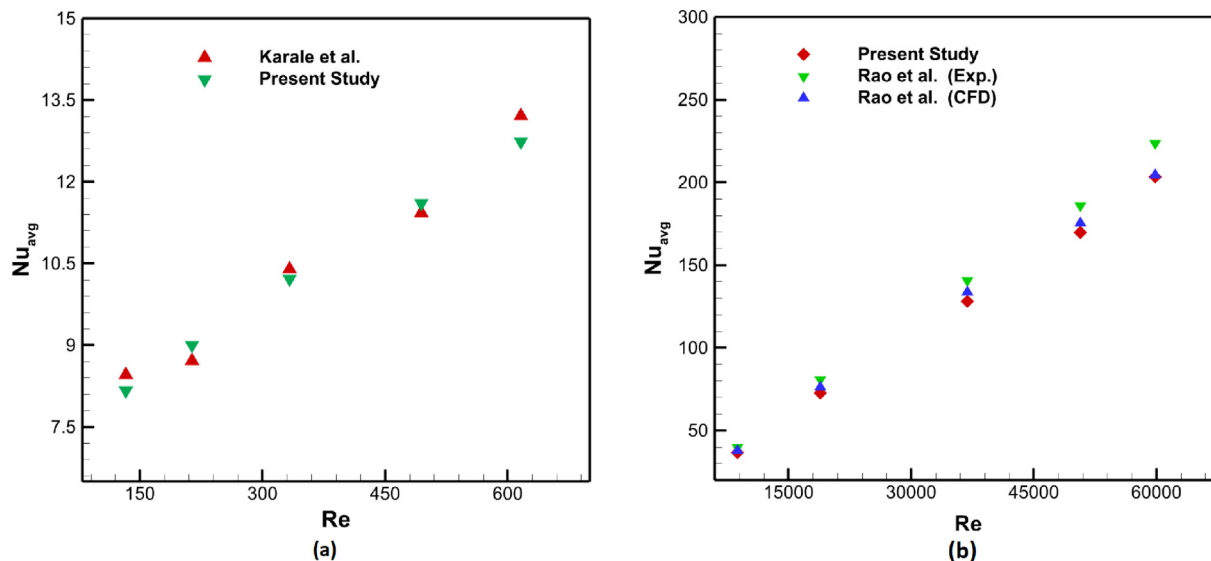


Fig. 3 Validation of the present study with (a) Karale et al. [85] for serpentine channel and (b) Rao et al. [86] for dimpled channel.

is evident that the heat transfer coefficient goes up as dimples are added to the computational domain. There are 12 dimples on one side of each turn making a total of 48 dimples in the test section. The dimples are arranged uniformly in a parallel arrangement with a spanwise (y/d) distance of 3.125 and a streamwise distance (x/d) is 11.25. The dimpled surface creates obstructions for fluids to flow, which increases the turbulence and makes heat transfer go up. Also, the dimpled face impacts the physical properties of the coolant because of the turbulence around dimple vicinities over a fluid pattern. As heat transmission is a surface phenomenon, the changes in the surface caused by dimple shapes aid in increasing the heat transfer as shown in Fig. 5 (a). Moreover, Fig. 7 clearly indicates that the temperature in the dimple wakes and at flow reattachments is lower than in other areas, whereas the temperatures in separation zones are higher. It signifies that the reattachment and the vortices produced from dimples generate a significant heat transfer zone. The vortices generated due to dimple effect and the flow separation and reattachment can be visualised from Fig. 4. Fig. 4 (a) shows the flow deviation due to dimples and vortex creation and Fig. 4 (b) shows the vortex created due to dimple effect. Fig. 4 (c) shows the flow separation and reattachment of flow along the dimple vicinity. The boundary layer separation causes a low heat transmission zone. A stronger heat transfer occurs in the upstream region of protrusions due to the flow impinging on the protrusion's front. However, when separation occurs, heat transmission decreases.

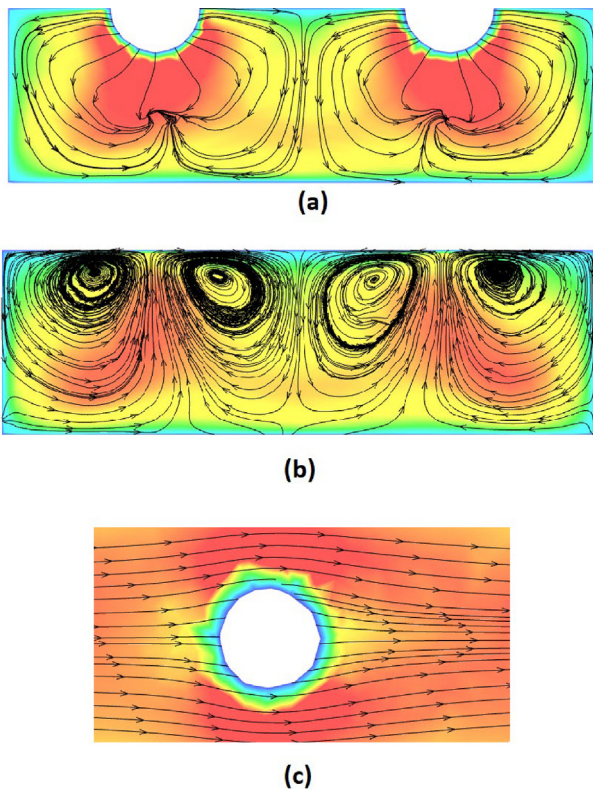


Fig. 4 (a) Vortex creation in dimple; (b) Vortex creation after dimple; (c) Flow separation and reattachment.

8.1.2. Pressure drop and friction factor

The investigation also compared the pressure losses and friction factors of the smooth and dimpled serpentine channels. There was a greater pressure drop and friction coefficient in the dimpled serpentine channel than in the smooth channel. Due to the obstructive nature of dimpled surfaces, the impact causes a rise in both the pressure drop and the friction coefficient. Velocity was decreased because of the obstructions caused by dimples, especially in the wake regions of the dimples. Fig. 5 (b) shows the pressure drop with respect to Re. Among the analyzed cases, the lowest average pressure drop was noticed for $Re\ 5 \times 10^3$ and the maximum pressure drop was recorded for $Re\ 20 \times 10^3$ for both cases. For $Re\ 5 \times 10^3$, the average pressure drop recorded for the smooth serpentine channel was 42.18 Pa whereas, for the dimpled serpentine channel, it was 71.69 Pa and for $Re\ 20 \times 10^3$, on average, about 397.71 Pa and 752.39 Pa.

8.1.3. Performance Evaluation Criterion (PECrs)

The Performance Evaluation Criterion (PEC) for the smooth serpentine channel and the dimpled serpentine channel were investigated using Equation (29). It evaluates the thermal performance by taking not only heat transfer enhancement but also pressure drop into account [87]. Fig. 5 (c) shows the PEC values for both types of channels. Since here PEC is calculated with respect to the smooth serpentine channel with water as a coolant by the aforementioned formula, any value above 1 is considered to have better thermal performance. For dimpled serpentine channel the PEC values obtained for Reynolds numbers 5×10^3 , 10×10^3 , 15×10^3 , and 20×10^3 were 2.47, 2.20, 1.99, and 1.84 respectively. These values indicate significantly better thermal efficiency for the dimpled serpentine channel as compared to the smooth channel.

$$PEC_{rs} = \frac{Nu_{rs}/Nu_{ss}}{(f_{rs}/f_{ss})^{1/3}} \quad (29)$$

8.2. Performance Evaluation of dimpled serpentine channel using Al_2O_3 -Cu nanofluid

Since the comparative study between the serpentine channel with smooth surface and dimpled surface concludes that the dimpled serpentine channel provides better thermal performance, for further heat transfer enhancement in passive technique, studies were conducted with the better-performing channel using Al_2O_3 -Cu hybrid nanofluid as the working fluid. For getting an overall comparison, investigations were carried out in the same Re numbers as before.

8.2.1. Analysis of velocity distribution

Fig. 6 (A) shows the velocity distribution for water in the dimpled channel at $Re\ 20 \times 10^3$ and Fig. 6 (B) shows the velocity distribution using nanofluid of 0.1%, 0.33%, 0.75%, and 1% volume fractions of Al_2O_3 -Cu at $Re\ 20 \times 10^3$. From the figure, it can be seen that maximum velocity was for 1% vol. Al_2O_3 -Cu followed by 0.75%, 0.33%, and 0.1% respectively and the lowest was observed for water in the smooth channel. Because of dimple protrusions, near the dimpled surfaces, secondary flow is induced. Since there are two dimples along the width of the channel there are two prominent regions of secondary

flow, aligned with the dimples. The fluid velocity near the dimples is higher and it can be explained by Bernoulli's principle. According to Bernoulli's principle, if the cross-sectional area decreases, the fluid velocity should increase to maintain continuity. Besides this, velocity close to the periphery is lower because of the boundary layer's effect. For the dimpled channel, albeit the velocity profiles for water and the nanofluids are alike qualitatively, however quantitatively, the velocity magnitudes of $\phi = 0.1\%$, 0.33% , 0.75% , and 1% nanofluid are not the same. The main reason for this variation is the difference in viscous forces and buoyancy. Moreover, more density and viscosity make the dynamic and thermal boundary layer for nanofluid thicker as compared to the base fluid water. As the

inclusion of $\text{Al}_2\text{O}_3\text{-Cu}$ nanoparticle is done to water for preparing the nanofluid, it makes the intermixing of the fluid layers better, consequently intensifying the induced secondary flow. This phenomenon leads to the conclusion that the more the incorporation of nanoparticles, the greater the velocity magnitude.

8.2.2. Temperature distribution analysis

Fig. 7 depicts the temperature changes along the smooth channel walls and the dimpled channel while using water and different concentrations of $\text{Al}_2\text{O}_3\text{-Cu}$ nanofluid as coolant at $\text{Re } 15 \times 10^3$. Fig. 7 shows the temperature contour taken at a distance of distance 0.285 m in the xy plane. It is observed that

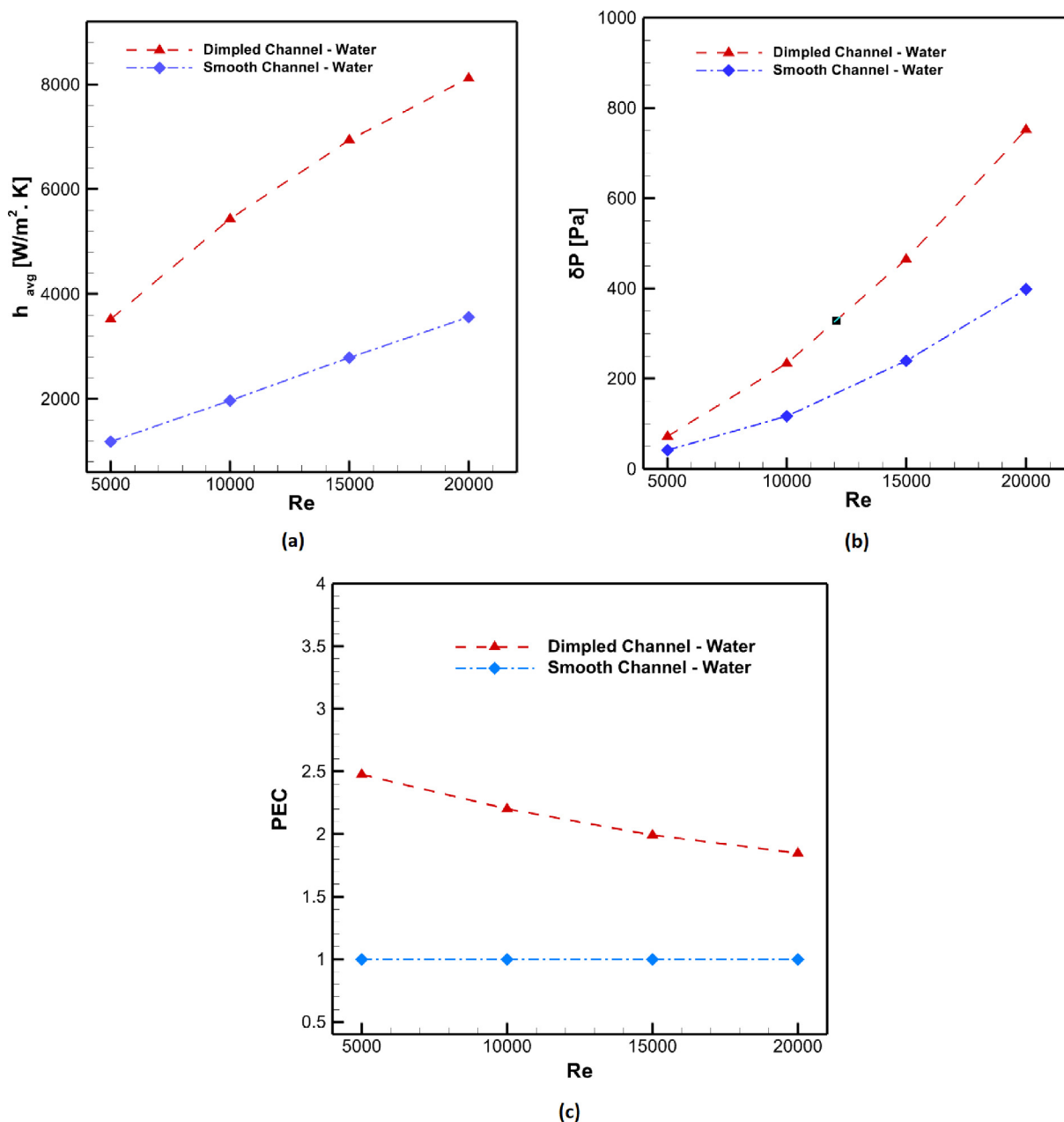


Fig. 5 Comparison between the smooth and the dimpled channel with water as coolant (a) Heat transfer coefficient, (b) Pressure drop, (c) PEC.

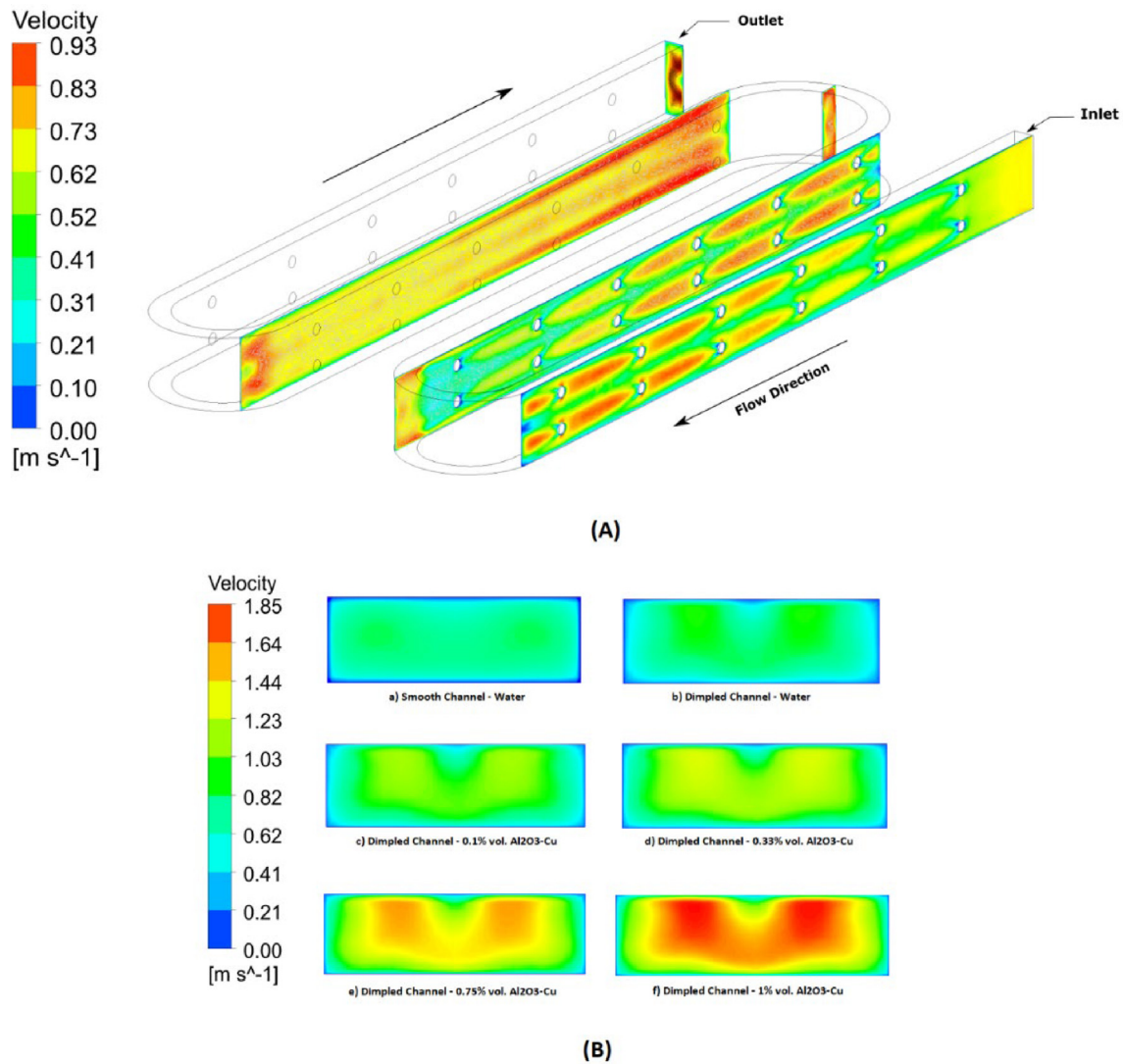


Fig. 6 Velocity distribution contour; (A) At various position of the channel, (B) Variation of flow velocity for different channels and nanofluid concentrations.

for the dimpled channel, as the concentrations of the nanofluid increase, thermo-physical characteristics of the working fluid get better. Consequently, the temperature of the wall of the channel decreases. The wall temperature obtained for 0.1 % vol. nanofluid is lower than for water, followed by 0.33% vol. and 0.75% vol. respectively, and the lowest temperature is obtained for 1 vol% nanofluid. As seen in the figure, the temperature of the wall of the channel with dimples was much lower than that of the channel without dimples. The lowest temperature was obtained in the dimpled channel with a 1% vol. concentration is 309.90 K at the surrounding areas of the dimples. The dimpled surface played a big part in lowering the temperature of the walls by causing secondary flow close to the dimples. In addition, dimpled surfaces hamper the boundary layer growth, which causes the intensity of the turbulent flow to rise. Increased Turbulent Intensity (TI) mostly made heat transfer better, which caused the wall temperature to drop. Nanofluid usage in the dimpled serpentine channel further improved the thermal performance of the heat exchanger. As a result, the temperature at the wall is reduced more as the nanofluid concentration is increased.

8.2.3. Turbulence intensity

Turbulence Intensity (TI) is a key factor in improving heat transfer. So, the higher the value of TI, the higher the value of the heat transfer coefficient would become. Fig. 8 shows the change in TI for the plain serpentine channel and dimpled serpentine channel with the base fluid water and then also with Al_2O_3 -Cu/water nanofluid with $\phi = 0.1\%, 0.33\%, 0.75\%$, and 1% at the dimple closest to the outlet (80 mm from the outlet) for the value of 20×10^3 Re. The value of turbulence intensity is found to be higher in the channel with dimpled walls than in a smooth channel, as the dimple jaggedness is significant for making more turbulence near the walls. Fig. 8 shows that the value of TI is maximum for 1% volume Al_2O_3 -Cu, then 0.75% vol., 0.33% vol. followed by 0.1% volume, and then the base fluid. TI is recorded lowest for the base fluid. It can be said that the characteristics of turbulence have the greatest impact on the presence of nanoparticles. So, when the volume fraction of nanofluid goes up, the value of TI is also increased. Also, the figure shows that the value of TI is highest near the dimples and walls of each case and it decreases

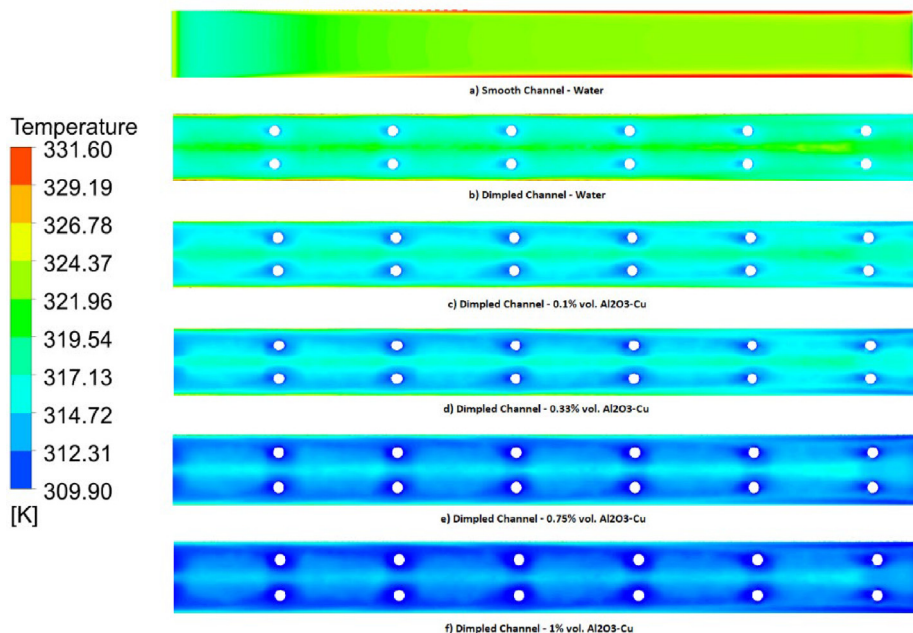


Fig. 7 Variation of temperature for different channels and nanofluid concentrations.

gradually away from the walls of the flow regime. The value of TI is lowest in the center of the fluid domain. Hence, it is quite evident that the introduction of dimpled protrusions readily increased the turbulence intensity and nanofluids corresponding to their concentration increased the TI even more.

Turbulence Intensity and viscosity ratio were kept at 5%. By increasing the turbulence intensity ratio to 10%, calculation was made for water at Re 20,000 in the dimpled channel. As the turbulence intensity is increased, the Nusselt number and pressure drop change are not significant. So 5% Turbulence intensity with specification method of Turbulence intensity and Viscosity ratio was considered for the present study.

8.2.4. Heat transfer enhancement

In Fig. 9 (a) Average Heat Transfer Coefficient (HTC) and Re are plotted along the y and x -axis to obtain the graphic comparison between the working fluids of this study by showing the variation of HTC as a function of Re . HTC was calculated using equation (22). From the figure, it is clear that 1% vol. Al_2O_3 -Cu nanofluid has the highest HTC as compared to other fluids. In the dimpled serpentine channel, the rate of heat transfer increased gradually with the increasing volume concentration of the nanofluid. In the dimpled serpentine channel, with respect to water, HTC increased 58.15% for Re 5×10^3 ,

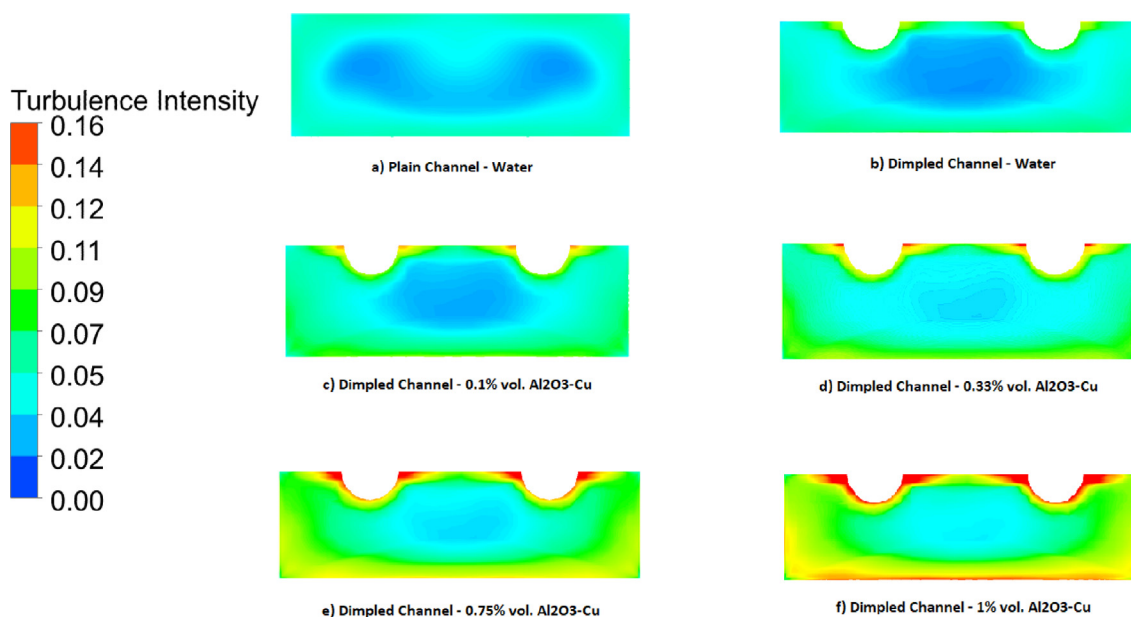


Fig. 8 Variation of turbulence intensity for different channels and nanofluid concentrations.

and for $Re\ 20 \times 10^3$, about a 226% increment has been recorded. Since the thermophysical characteristics like thermal conductivity, viscosity, etc. of the coolants were enhanced when nanoparticles with greater thermal conductivities were added to the base fluid, the improvement in heat transfer could be seen. As a consequence of the enhanced thermal conductivity, nanofluids are capable of enhancing the coefficient of heat transfer. Moreover, the same fluid has a better heat transfer rate for higher Re . For 1% Al_2O_3 -Cu, the heat transfer rate almost doubled from $5.57\ kW/m^2 \cdot K$ to $11.51\ kW/m^2 \cdot K$ for $Re\ 5 \times 10^3$ to $Re\ 20 \times 10^3$. Fluid flow with a higher Re experiences more turbulence than that of lower Re flows which ensure significant mixing of the boundary layer and the bulk fluid. This eventually increases the heat transfer rate. However, the rate of increase of HTC with Re gradually decreases with the increment of Re .

Abed et al. [88] obtained a 158% increment in heat transfer with 30/70% glycerine/water fluid in a serpentine channel. The Prandtl number obtained for this working fluid was 137. Awais

et al. [21] compared different types of varied section lengths in serpentine channels and obtained 50% enhancement in heat transfer rate with 5% Al_2O_3 / Water nanofluid. The result obtained in the present study is significantly better than that of results obtained in the dimpled channels studied by Rao et al. [86] and Ahmed et al. [14]. The findings of some of the studies are tabulated in Table 3.

8.2.5. Pressure drop

The addition of nanoparticles increases the coolant's thermal conductivity, as explained before. Nonetheless, the addition of nanoparticles increases viscosity and density, leading to pressure drop increment.

Fig. 9 (b) illustrates the average pressure decrease for each of the analyzed scenarios when Re is varied. Compared to a smooth serpentine channel, a dimpled serpentine channel exhibits a greater pressure drop owing to the obstructions caused by dimpled protrusions on the surfaces of the fluid's motion. In addition, the figure demonstrates that the addition of

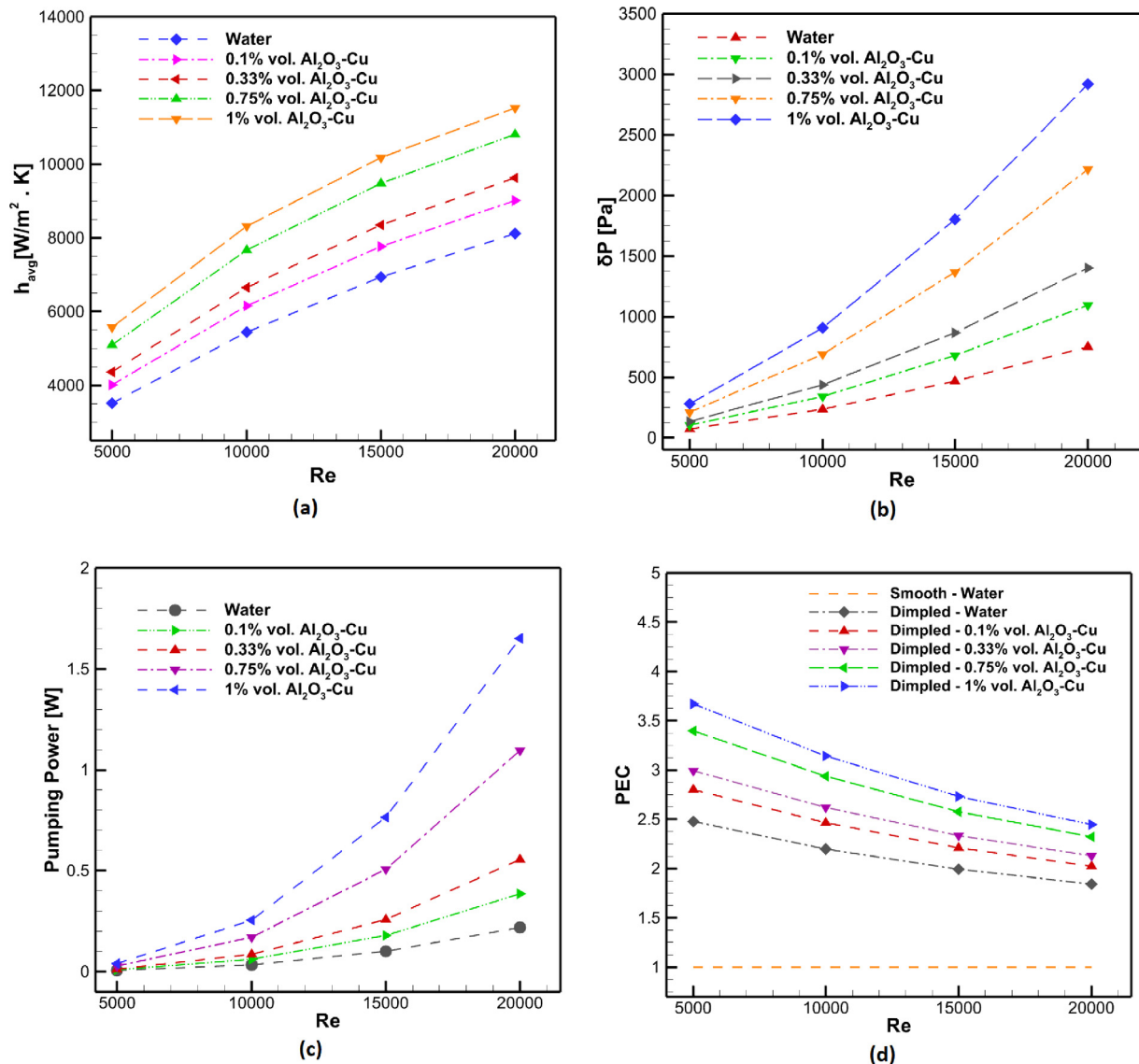


Fig. 9 Comparison of water and various concentrations of Al_2O_3 -Cu nanofluid.

Table 3 Comparison of results with other similar studies.

Author	Channel type	Technique	Nanofluid used	Case	Results
Present Study	Serpentine	Numerical	1% Al ₂ O ₃ -Cu/Water	Re 5000	368.90% increment in heat transfer
Abed et al.[88]	Serpentine	Experimental	30/70% glycerine/water	Pr 137	158% increment in heat transfer
Awais et al.[21]	Serpentine	Numerical	5% Al ₂ O ₃ / Water	5 L/min Volumetric Flow	50% increment in heat transfer
Rao et al.[86]	Dimpled	Experimental	Water	Re 8500	28% increment in heat transfer
Ahmed et al.[14]	Dimpled	Numerical	4% Al ₂ O ₃ / Water	Re 1000	32% increment in thermal efficiency

nanoparticles raised the average pressure drop. Because of the increased cohesions among nanoparticles, as the weight concentration rises, the average pressure drop increases gradually. Therefore, 1% vol. Al₂O₃-Cu nanofluid exhibited the maximum pressure loss, which gradually reduced and reached its minimum value for the base fluid. Furthermore, as can be seen in Fig. 9 (b), for a particular nanofluid the pressure drop rises as Re increases. Since the rise in Re causes an increase in the hydrodynamic entry length, the velocity gradient and shear stress at the entrance length's wall area increase. Consequently, the pressure drops increase in the entry area, which causes the average pressure drop to rise as Re increases.

$$\text{Pumping Power} = \frac{\pi}{4} \cdot D_h \cdot v \cdot \Delta P \quad (30)$$

Equation (30) was used to calculate the pumping power [10]. The pumping power is shown in Fig. 9 (c) as a function of Re. The nanofluid containing 1% Al₂O₃-Cu has the maximum pumping power, which falls with decreasing weight concentrations, while the smooth channel has the lowest pumping power among all.

8.2.6. Performance Evaluation Criterion (PEC_{nf})

As discussed, pressure drop and heat transfer are both higher in the dimpled serpentine channel than in the smooth serpentine channel. Since pressure drop is intrinsically tied to pumping power and the effectiveness of cost, as the pressure drop goes up, the amount of pumping power needed goes up as well. So, to figure out how well the geometry works, the thermal efficiency of the dimpled surface was measured using the Performance Evaluation Criterion (PEC), which is shown in Equation (31) [73,87]. For thermal efficiency, PEC looks at both the case where heat transfer improves and the case where the pressure drops. Also, just like with a rough-surfaced dimpled channel, adding nanoparticles to the base fluid water, increases the heat transfer at a cost of a drop in pressure. In order to put the nanofluid to use, the conclusion needs to take not only the rise in heat transfer but also the decrease in pressure into consideration. Using the Performance Evaluation Criterion or Thermal Performance Factor (TPF) for nanofluids [78,89,90], the thermal performance of nanofluids was measured using Equation (31).

$$PEC_{nf} = \frac{Nu_{nf}/Nu_{bf}}{(f_{nf}/f_{bf})^{1/3}} \quad (31)$$

If the PEC value is higher than 1, it is clear that improvement in heat transfer is more than pressure loss. If, on the other hand, the PEC value is lower than 1, it means that pressure loss is greater than heat transfer improvement. The thermal performance for all the cases studied with different Reynolds numbers is shown in Fig. 9 (d). As seen in the figure,

the PEC values for each case of a dimpled channel are all higher than 1. In addition to that, it is also evident from the figure that based on thermos-hydraulic performance, a heat exchanger with a dimpled serpentine channel would be better than one with a smooth serpentine channel. When compared to the smooth serpentine channel, the maximum PEC value of 1.47 for the dimpled channel was reached at Re 5×10^3 , which was achieved by utilizing water as the coolant. It was observed that as Re went up, the value of PEC went down, and the minimum improvement in thermal performance was found to be 84.51% at Re 20×10^3 . With higher volume concentrations, the thermal efficiency of Al₂O₃-Cu/water nanofluid in the dimpled serpentine channel got better. Consequently, 1% Al₂O₃-Cu nanofluid had the best thermal performance, followed by 0.75%, 0.33%, and base fluid, which had the worst performance. For $\phi = 1\%$ Al₂O₃-Cu, the thermal performance went up by a maximum of 267.04%, which is an outstanding improvement in terms of the distinctiveness of the investigations done. It was noted that the maximum increase in thermal performance was 239.67%, 199.18%, and 179.93% for $\phi = 0.75\%$, 0.33%, and 0.1% Al₂O₃-Cu nanofluid, respectively at Re 5×10^3 . This is a remarkable as well as recognizable improvement in thermal performance for industrial applications.

From the discussion, it is clear that as Re went up, the value of PEC went down, and for all of the cases that were investigated, Re 5×10^3 was the highest value of PEC found. So, the discussion leads to the conclusion that a dimpled serpentine channel with base fluid water and nanofluids of different concentrations will work better at lower ranges of Re in a turbulent flow regime.

9. Conclusion

This study investigates the thermos-hydraulic performance of a serpentine channel with three steps passive heat transfer enhancement technique. A serpentine channel surface is modified by introducing dimples and Al₂O₃-Cu/water hybrid nanofluid is used as the working fluid for obtaining better thermal efficiency in turbulent flow regimes. The following conclusions are reached while performing this study.

- At first, using only the base fluid water, with respect to the smooth serpentine channel, for the dimpled channel, about 147.62% increment in thermal efficiency is obtained at Re 5×10^3 . This is the highest improvement for the base fluid among the test cases for four different Reynolds numbers. As the Re increases, the improvement in PEC gradually decreases. 120.01%, 99.29%, and 84.51% increment in performance are obtained for Re 10×10^3 , 15×10^3 , and 20×10^3 respectively.

- Further investigations of the dimpled serpentine channel with four different concentrations of Al_2O_3 -Cu/water hybrid nanofluid reveal that the heat transfer performance is improved by 267.04%, 239.67%, 199.18%, and 179.93% for $\phi = 1\%$, 0.75%, 0.33% and 0.1% volume concentrations respectively at $\text{Re } 5 \times 10^3$. For nanofluid working medium too, the rate of thermal performance enhancement reduces with an increase in Re. However, the values of PEC which are obtained in the study after modifications and changing heat transfer medium fluid are extraordinary.
- The heat transfer performance improves at a pressure drop cost; thus, higher pumping power is required.

So, the investigation findings suggest that 1% vol. Al_2O_3 -Cu/water hybrid nanofluid with the dimpled surfaced serpentine channel will provide the best performance in terms of heat transfer enhancement among all the test cases. For lower Re, the comparative improvement is more as compared to higher Re.

Declaration of Competing Interest

The authors declare that they have no known competing financial interests or personal relationships that could have appeared to influence the work reported in this paper.

References

- [1] J. Raza, F. Mebarek-Oudina, A.J. Chamkha, Magnetohydrodynamic flow of molybdenum disulfide nanofluid in a channel with shape effects, *Multidiscip. Model. Mater. Struct.* (2019).
- [2] F. Selimefendigil, H.F. Öztop, A.J. Chamkha, Role of magnetic field on forced convection of nanofluid in a branching channel, *Int. J. Numer. Meth. Heat Fluid Flow* (2019).
- [3] A.J. Chamkha, On laminar hydromagnetic mixed convection flow in a vertical channel with symmetric and asymmetric wall heating conditions, *Int. J. Heat Mass Transf.* 45 (12) (2002) 2509–2525.
- [4] S. Alzahrani, S. Usman, CFD simulations of the effect of in-tube twisted tape design on heat transfer and pressure drop in natural circulation, *Therm. Sci. Eng. Progr.* 11 (2019) 325–333.
- [5] S.P. Nalavade, C.L. Prabhune, N.K. Sane, Effect of novel flow divider type turbulators on fluid flow and heat transfer, *Therm. Sci. Eng. Progr.* 9 (2019) 322–331.
- [6] A. Bhattad, J. Sarkar, P. Ghosh, Hydrothermal performance of different alumina hybrid nanofluid types in plate heat exchanger, *J. Therm. Anal. Calorim.* 139 (6) (2020) 3777–3787.
- [7] R.K. Ajeel, K. Sopian, R. Zulkifli, A novel curved-corrugated channel model: Thermal-hydraulic performance and design parameters with nanofluid, *Int. Commun. Heat Mass Transfer* 120 (2021) 105037.
- [8] R.K. Ajeel, K. Sopian, R. Zulkifli, Thermal-hydraulic performance and design parameters in a curved-corrugated channel with L-shaped baffles and nanofluid, *J. Storage Mater.* 34 (2021) 101996.
- [9] R.K. Ajeel et al, Numerical investigation of binary hybrid nanofluid in new configurations for curved-corrugated channel by thermal-hydraulic performance method, *Powder Technol.* 385 (2021) 144–159.
- [10] F. Ahmed et al, Assessment of thermo-hydraulic performance of MXene-based nanofluid as coolant in a dimpled channel: a numerical approach, *J. Therm. Anal. Calorim.* 147 (22) (2022) 12669–12692.
- [11] M. Keimanesh et al, Study of a third grade non-Newtonian fluid flow between two parallel plates using the multi-step differential transform method, *Comput. Math. Appl.* 62 (8) (2011) 2871–2891.
- [12] R.K. Ajeel et al, Assessment and analysis of binary hybrid nanofluid impact on new configurations for curved-corrugated channel, *Adv. Powder Technol.* 32 (10) (2021) 3869–3884.
- [13] R.K. Ajeel, W.-I. Salim, K. Hasnan, Design characteristics of symmetrical semicircle-corrugated channel on heat transfer enhancement with nanofluid, *Int. J. Mech. Sci.* 151 (2019) 236–250.
- [14] F. Ahmed et al, The impact of D-shaped jaggedness on heat transfer enhancement technique using Al_2O_3 based nanoparticles, *Int. J. Thermofluids* 10 (2021) 100069.
- [15] F. Ahmed et al, Numerical investigation of the thermo-hydraulic performance of water-based nanofluids in a dimpled channel flow using Al_2O_3 , CuO, and hybrid Al_2O_3 -CuO as nanoparticles, *Heat Transfer* 50 (5) (2021) 5080–5105.
- [16] R.K. Ajeel, W.-I. Salim, K. Hasnan, Experimental and numerical investigations of convection heat transfer in corrugated channels using alumina nanofluid under a turbulent flow regime, *Chem. Eng. Res. Des.* 148 (2019) 202–217.
- [17] R.K. Ajeel, W.-I. Salim, K. Hasnan, Thermal performance comparison of various corrugated channels using nanofluid: Numerical study, *Alex. Eng. J.* 58 (1) (2019) 75–87.
- [18] R.K. Ajeel, W.-I. Salim, K. Hasnan, Numerical investigations of heat transfer enhancement in a house shaped-corrugated channel: Combination of nanofluid and geometrical parameters, *Therm. Sci. Eng. Progr.* 17 (2020) 100376.
- [19] A. Bhattad, J. Sarkar, P. Ghosh, Improving the performance of refrigeration systems by using nanofluids: A comprehensive review, *Renew. Sustain. Energy Rev.* 82 (2018) 3656–3669.
- [20] J.C. Umavathi et al, Unsteady two-fluid flow and heat transfer in a horizontal channel, *Heat Mass Transf.* 42 (2) (2005) 81–90.
- [21] M. Awais et al, Computational assessment of Nano-particulate (Al_2O_3 /Water) utilization for enhancement of heat transfer with varying straight section lengths in a serpentine tube heat exchanger, *Therm. Sci. Eng. Progr.* 20 (2020) 100521.
- [22] M. Awais et al, Heat transfer and pressure drop performance of Nanofluid: A state-of-the-art review, *Int. J. Thermofluids* 9 (2021) 100065.
- [23] R.K. Ajeel et al, Analysis of thermal-hydraulic performance and flow structures of nanofluids across various corrugated channels: An experimental and numerical study, *Therm. Sci. Eng. Progr.* 19 (2020) 100604.
- [24] A. Bhattad, J. Sarkar, P. Ghosh, Exergetic analysis of plate evaporator using hybrid nanofluids as secondary refrigerant for low-temperature applications, *Int. J. Exergy* 24 (1) (2017) 1–20.
- [25] M. VeeraKrishna, G. Subba Reddy, A. Chamkha, Hall effects on unsteady MHD oscillatory free convective flow of second grade fluid through porous medium between two vertical plates, *Phys. Fluids* 30 (2) (2018) 023106.
- [26] A.J. Chamkha, Flow of two-immiscible fluids in porous and nonporous channels, *J. Fluids Eng.* 122 (1) (2000) 117–124.
- [27] A. Dogonchi et al, Numerical simulation of hydrothermal features of Cu-H₂O nanofluid natural convection within a porous annulus considering diverse configurations of heater, *J. Therm. Anal. Calorim.* 141 (5) (2020) 2109–2125.
- [28] A.M. Bayomy, M. Saghir, Experimental study of using γ - Al_2O_3 -water nanofluid flow through aluminum foam heat sink: comparison with numerical approach, *Int. J. Heat Mass Transf.* 107 (2017) 181–203.
- [29] M. Goodarzi et al, Investigation of heat transfer and pressure drop of a counter flow corrugated plate heat exchanger using

- MWCNT based nanofluids, *Int. Commun. Heat Mass Transfer* 66 (2015) 172–179.
- [30] M. Goodarzi et al, Investigation of heat transfer performance and friction factor of a counter-flow double-pipe heat exchanger using nitrogen-doped, graphene-based nanofluids, *Int. Commun. Heat Mass Transfer* 76 (2016) 16–23.
- [31] M. Akhavan-Behabadi et al, An experimental investigation on rheological properties and heat transfer performance of MWCNT-water nanofluid flow inside vertical tubes, *Appl. Therm. Eng.* 106 (2016) 916–924.
- [32] A.J. Chamkha, T. Groşan, I. Pop, Fully developed free convection of a micropolar fluid in a vertical channel, *Int. Commun. Heat Mass Transfer* 29 (8) (2002) 1119–1127.
- [33] J.P. Kumar et al, Fully-developed free-convective flow of micropolar and viscous fluids in a vertical channel, *App. Math. Model.* 34 (5) (2010) 1175–1186.
- [34] M. Khoshvaght-Aliabadi, A. Alizadeh, An experimental study of Cu–water nanofluid flow inside serpentine tubes with variable straight-section lengths, *Exp. Therm Fluid Sci.* 61 (2015) 1–11.
- [35] A. Feizabadi, M. Khoshvaght-Aliabadi, A.B. Rahimi, Numerical investigation on Al₂O₃/water nanofluid flow through twisted-serpentine tube with empirical validation, *Appl. Therm. Eng.* 137 (2018) 296–309.
- [36] W.M. Abed et al, Experimental investigation of the impact of elastic turbulence on heat transfer in a serpentine channel, *J. Nonnewton. Fluid Mech.* 231 (2016) 68–78.
- [37] R.K. Ajeel et al, Turbulent convective heat transfer of silica oxide nanofluid through corrugated channels: An experimental and numerical study, *Int. J. Heat Mass Transf.* 145 (2019) 118806.
- [38] R.K. Ajeel, W.-I. Salim, K. Hasnan, Influences of geometrical parameters on the heat transfer characteristics through symmetry trapezoidal-corrugated channel using SiO₂-water nanofluid, *Int. Commun. Heat Mass Transfer* 101 (2019) 1–9.
- [39] G. Huminic, A. Huminic, Heat transfer and entropy generation analyses of nanofluids in helically coiled tube-in-tube heat exchangers, *Int. Commun. Heat Mass Transfer* 71 (2016) 118–125.
- [40] A. Perwez, S. Shende, R. Kumar, Heat transfer and friction factor characteristic of spherical and inclined teardrop dimple channel subjected to forced convection, *Exp. Heat Transfer* 32 (2) (2019) 159–178.
- [41] J. Chen, H. Müller-Steinhagen, G.G. Duffy, Heat transfer enhancement in dimpled tubes, *Appl. Therm. Eng.* 21 (5) (2001) 535–547.
- [42] A. García et al, The influence of artificial roughness shape on heat transfer enhancement: Corrugated tubes, dimpled tubes and wire coils, *Appl. Therm. Eng.* 35 (2012) 196–201.
- [43] A. Bhattad, J. Sarkar, Hydrothermal performance of plate heat exchanger with an alumina–graphene hybrid nanofluid: experimental study, *J. Braz. Soc. Mech. Sci. Eng.* 42 (7) (2020) 1–10.
- [44] A. Bhattad, Exergy analysis of plate heat exchanger with graphene alumina hybrid nanofluid: experimentation, *Int. J. Exergy* 33 (3) (2020) 254–262.
- [45] P. Kumar et al, Experimental investigation of heat transfer enhancement and fluid flow characteristics in a protruded surface heat exchanger tube, *Exp. Therm Fluid Sci.* 71 (2016) 42–51.
- [46] A. Bhattad, J. Sarkar, P. Ghosh, Energy-economic analysis of plate evaporator using brine-based hybrid nanofluids as secondary refrigerant, *Int. J. Air-Condition. Refrigerat.* 26 (01) (2018) 1850003.
- [47] A. Bhattad, J. Sarkar, P. Ghosh, Energetic and exergetic performances of plate heat exchanger using brine-based hybrid nanofluid for milk chilling application, *Heat Transfer Eng.* (2019).
- [48] A. Bhattad, J. Sarkar, P. Ghosh, Experimentation on effect of particle ratio on hydrothermal performance of plate heat exchanger using hybrid nanofluid, *Appl. Therm. Eng.* 162 (2019) 114309.
- [49] A. Bhattad, Experimental investigation of Al₂O₃–MgO hot hybrid nanofluid in a plate heat exchanger, *Heat Transfer* 49 (4) (2020) 2344–2354.
- [50] S. Parvin et al, Thermal conductivity variation on natural convection flow of water–alumina nanofluid in an annulus, *Int. J. Heat Mass Transf.* 55 (19–20) (2012) 5268–5274.
- [51] L.S. Sundar et al, Hybrid nanofluids preparation, thermal properties, heat transfer and friction factor—a review, *Renew. Sustain. Energy Rev.* 68 (2017) 185–198.
- [52] R.L. Hamilton, O.K. Crosser, Thermal conductivity of heterogeneous two-component systems, *Ind. Eng. Chem. Fundamen.* 1 (3) (1962) 187–191.
- [53] B. Takabi, H. Shokouhmand, Effects of Al₂O₃–Cu/water hybrid nanofluid on heat transfer and flow characteristics in turbulent regime, *Int. J. Mod. Phys. C* 26 (04) (2015) 1550047.
- [54] S. Suresh et al, Synthesis of Al₂O₃–Cu/water hybrid nanofluids using two step method and its thermo physical properties, *Colloids Surf. A Physicochem. Eng. Asp.* 388 (1–3) (2011) 41–48.
- [55] M. Saghir, M. Rahman, Forced convection of Al₂O₃–Cu, TiO₂–SiO₂, FWCNT–Fe₃O₄, and ND–Fe₃O₄ hybrid nanofluid in porous media, *Energies* 13 (11) (2020) 2902.
- [56] L.S. Sundar, M.K. Singh, A.C. Sousa, Enhanced heat transfer and friction factor of MWCNT–Fe₃O₄/water hybrid nanofluids, *Int. Commun. Heat Mass Transfer* 52 (2014) 73–83.
- [57] L.S. Sundar et al, Nanodiamond-Fe₃O₄ nanofluids: preparation and measurement of viscosity, electrical and thermal conductivities, *Int. Commun. Heat Mass Transfer* 73 (2016) 62–74.
- [58] Y. Xuan, W. Roetzel, Conceptions for heat transfer correlation of nanofluids, *Int. J. Heat Mass Transf.* 43 (19) (2000) 3701–3707.
- [59] S. Lee, et al., Measuring thermal conductivity of fluids containing oxide nanoparticles, 1999.
- [60] S.E.B. Maiga et al, Heat transfer enhancement by using nanofluids in forced convection flows, *Int. J. Heat Fluid Flow* 26 (4) (2005) 530–546.
- [61] D. Toghraie et al, Two-phase investigation of water–Al₂O₃ nanofluid in a micro concentric annulus under non-uniform heat flux boundary conditions, *Int. J. Numer. Meth. Heat Fluid Flow* (2019).
- [62] A.J. Chamkha, Unsteady laminar hydromagnetic fluid–particle flow and heat transfer in channels and circular pipes, *Int. J. Heat Fluid Flow* 21 (6) (2000) 740–746.
- [63] A. Albojamal, K. Vafai, Analysis of single phase, discrete and mixture models, in predicting nanofluid transport, *Int. J. Heat Mass Transf.* 114 (2017) 225–237.
- [64] R. Kandasamy, N.A. bt Adnan, R. Mohammad, Nanoparticle shape effects on squeezed MHD flow of water based Cu, Al₂O₃ and SWCNTs over a porous sensor surface, *Alexandria Eng. J.*, 2018. 57(3): p. 1433-1445.
- [65] A.J. Chamkha, Hydromagnetic two-phase flow in a channel, *Int. J. Eng. Sci.* 33 (3) (1995) 437–446.
- [66] D. Kim et al, Convective heat transfer characteristics of nanofluids under laminar and turbulent flow conditions, *Curr. Appl Phys.* 9 (2) (2009) e119–e123.
- [67] D. Wen, Y. Ding, Experimental investigation into convective heat transfer of nanofluids at the entrance region under laminar flow conditions, *Int. J. Heat Mass Transf.* 47 (24) (2004) 5181–5188.
- [68] T. Armaghani et al, MHD mixed convection of localized heat source/sink in an Al₂O₃–Cu/water hybrid nanofluid in L-shaped cavity, *Alex. Eng. J.* 60 (3) (2021) 2947–2962.

- [69] L. Kolsi et al, Numerical investigation of combined buoyancy-thermocapillary convection and entropy generation in 3D cavity filled with Al₂O₃ nanofluid, *Alex. Eng. J.* 56 (1) (2017) 71–79.
- [70] M. Awais et al, Synthesis, heat transport mechanisms and thermophysical properties of nanofluids: A critical overview, *Int. J. Thermofluids* 10 (2021) 100086.
- [71] F. Ahmed et al, Computational assessment of thermo-hydraulic performance of Al₂O₃-water nanofluid in hexagonal rod-bundles subchannel, *Prog. Nucl. Energy* 135 (2021) 103700.
- [72] M. Izadi, A. Behzadmehr, D. Jalali-Vahida, Numerical study of developing laminar forced convection of a nanofluid in an annulus, *Int. J. Therm. Sci.* 48 (11) (2009) 2119–2129.
- [73] A. Kumar, R. Maithani, A.R.S. Suri, Numerical and experimental investigation of enhancement of heat transfer in dimpled rib heat exchanger tube, *Heat Mass Transf.* 53 (12) (2017) 3501–3516.
- [74] G. Yadigaroglu et al, Trends and needs in experimentation and numerical simulation for LWR safety, *Nucl. Eng. Des.* 221 (1–3) (2003) 205–223.
- [75] M. Rahimi-Esbo, Y. Vazifeshenas, Comparison of thermo-hydraulic performance of nanofluids and mixing vanes in a triangular fuel rod bundle, *J. Brazil. Soc. Mech. Sci. Eng.* 37 (1) (2015) 173–186.
- [76] I. Fluent et al, *Fluent 6.3 user's guide*, Fluent documentation, 2006, 2006.
- [77] H.E. Ahmed, B. Salman, A.S. Kerbeet, Heat transfer enhancement of turbulent forced nanofluid flow in a duct using triangular rib, *Int. J. Heat Mass Transf.* 134 (2019) 30–40.
- [78] F. Ahmed et al, Thermohydraulic performance of water mixed Al₂O₃, TiO₂ and graphene-oxide nanoparticles for nuclear fuel triangular subchannel, *Therm. Sci. Eng. Progr.* 24 (2021) 100929.
- [79] V. Yakhot, S.A. Orszag, Renormalization group analysis of turbulence. I. Basic theory, *J. Sci. Comput.* 1 (1) (1986) 3–51.
- [80] H.K. Versteeg, W. Malalasekera, *An introduction to computational fluid dynamics: the finite volume method*, Pearson education, 2007.
- [81] K. Benaissa et al, Predicting initial erosion during the hole erosion test by using turbulent flow CFD simulation, *App. Math. Model.* 36 (8) (2012) 3359–3370.
- [82] V. Bianco, O. Manca, S. Nardini, Performance analysis of turbulent convection heat transfer of Al₂O₃ water-nanofluid in circular tubes at constant wall temperature, *Energy* 77 (2014) 403–413.
- [83] F. Dittus, L. Boelter, Heat transfer in automobile radiators of the tubular type, *Int. Commun. Heat Mass Transfer* 12 (1) (1985) 3–22.
- [84] R. Maithani, A. Kumar, Correlations development for Nusselt number and friction factor in a dimpled surface heat exchanger tube, *Exp. Heat Transfer* 33 (2) (2020) 101–122.
- [85] C.M. Karale, S.S. Bhagwat, V.V. Ranade, Flow and heat transfer in serpentine channels, *AIChE J.* 59 (5) (2013) 1814–1827.
- [86] Y. Rao et al, Experimental and numerical study of heat transfer and flow friction in channels with dimples of different shapes, *J. Heat Transfer* 137 (3) (2015).
- [87] M. Lewis, Optimising the thermohydraulic performance of rough surfaces, *Int. J. Heat Mass Transf.* 18 (11) (1975) 1243–1248.
- [88] W.M. Abed et al, Numerical and experimental investigation of heat transfer and fluid flow characteristics in a micro-scale serpentine channel, *Int. J. Heat Mass Transf.* 88 (2015) 790–802.
- [89] A. Bhattad, J. Sarkar, Effects of nanoparticle shape and size on the thermohydraulic performance of plate evaporator using hybrid nanofluids, *J. Therm. Anal. Calorim.* 143 (1) (2021) 767–779.
- [90] A. Bhattad, J. Sarkar, P. Ghosh, Heat transfer characteristics of plate heat exchanger using hybrid nanofluids: effect of nanoparticle mixture ratio, *Heat Mass Transf.* 56 (8) (2020) 2457–2472.